UNIVERSITAT POLITÈCNICA
DE CATALUNYA
BARCELONATECH

UPCommons

Portal del coneixement obert de la UPC

http://upcommons.upc.edu/e-prints

Leonardo Marin, Andres Tarrasó, Ignacio Candela, Pedro Rodríguez. (2018) Stability analysis of a grid-connected VSC controlled by SPC. 7th International Conference on Renewable Energy Research and Applications : Paris, F rance , Oct. 14 - 17, 2018, 2018: IEEE, 2018. Pp. 1209-1214 Doi: 10.1109/ICRERA.2018.8567018.

© 2018 IEEE. Es permet l'ús personal d'aquest material. S'ha de demanar permís a l'IEEE per a qualsevol altre ús, incloent la reimpressió/reedició amb fins publicitaris o promocionals, la creació de noves obres col·lectives per a la revenda o redistribució en servidors o llistes o la reutilització de parts d'aquest treball amb drets d'autor en altres treballs.

UNIVERSITAT POLITÈCNICA
DE CATALUNYA
BARCELONATECH

Leonardo Marin, Andres Tarrasó, Ignacio Candela, Pedro Rodríguez. (2018) Stability analysis of a grid-connected VSC controlled by SPC. 7th International Conference on Renewable Energy Research and Applications : Paris, F rance , Oct. 14 - 17, 2018, 2018: IEEE, 2018. Pp. 1209-1214 Doi: 10.1109/ICRERA.2018.8567018.

© 2018 IEEE. Personal use of this material is permitted. Permission from IEEE must be obtained for all other users, including reprinting/ republishing this material for advertising or promotional purposes, creating new collective works for resale or redistribution to servers or lists, or reuse of any copyrighted components of this work in other works.

Stability Analysis of a Grid-Connected VSC Controlled by SPC

Leonardo Marin, Andres Tarrasó, Ignacio Candela
Department of Electrical Engineering
Technical University of Catalonia
GAIA Building, Terrassa, Barcelona, Spain 08222
Email: leonardo.marin@upc.edu

Pedro Rodriguez
Universidad de Loyola
Sevilla, SPAIN
Email: prodriguez@uloyola.es

***Abstract*—In the near future a large part of traditional generation based on conventional synchronous machines (SM) will be replaced by renewable generation based on voltage source converters (VSC).**

In this sense, power system operators have begun to demand VSC-based power plants be able to participate in the frequency and voltage regulation, and are also interested in services like inertia emulation and damping of power oscillation, functions that today are carried out by large synchronous generators. Therefore, several studies have suggested new ways to control voltage source converters, that try to emulate the behavior of synchronous generators and are known generically as Virtual Synchronous Machines.

The synchronous power controller (SPC) is a flexible solution that emulates the classical swing equation of a synchronous machine and improves its response. The SPC inherits the advantages of conventional synchronous generators, while it fixes many of its drawbacks.

In this work, a sensitivity analysis of a VSC connected to the grid and controlled by SPC is performed. In this sense, a non-linear mathematical model of the system is first developed. This non-linear model is then linearized, obtaining a linear model from which the eigenvalues and sensitivities of the system to some relevant parameters are calculated. Finally, time-domain simulations are performed to confirm the results of the sensitivity analysis.

***Index Terms*—small signal stability, synchronous power controller, state-space, eigenvalues, sensitivity analysis.**

I. Introduction

In recent decades, environmental issues and the continuous increase in oil prices have led to a rapid growth in the use of alternative energies, mainly solar and wind, and it is expected that this trend will accentuate in the coming years [1]. Nevertheless, due to its peculiar characteristics, integration of renewables into power systems is generally not possible without using the suitable power converters for controlling variables such as voltage en frequency [2].

Electrical systems are undergoing a rapid transition from synchronous machines (SM)-based systems to power converter-based systems in which voltage source converters (VSC) will play a key role. In this sense, many regulatory communities and system operators in the power sector have established grid codes to ensure proper connection of these renewable sources [3]. Participation in the frequency and voltage regulation, and services like inertia emulation and damping of power oscillation are well established in these grid codes [4, 5].

Therefore, several studies have suggested new ways to control VSCs, known generically as virtual synchronous machines (VSM) [6–8]. The idea underlying the VSM concept is to control the VSC by emulating the essential behaviour of a true SM [9]. In [8] a classification of VSMs is presented.

Synchronous power controller (SPC) presented in [10] is a flexible solution that inherits the advantages of conventional synchronous generators, while it fixes many of its drawbacks [11].

The electromechanical interaction of a SPC-controlled VSC is implemented through the emulation of the classical swing equation of SM, which enables adjusting the parameters of inertia and the damping according to the operating conditions to achieve an optimal response.

In addition, as in real SMs, SPC has an inherent power-based synchronization mechanism that provides the VSC the phase-angle to properly synchronize it with the main electrical grid. No additional synchronization method such as phase-locked loop (PLL) is necessary [12], which enables the VSC to operate in multiple scenarios including weak grids, as well as on electrical islands [13].

Regarding the electromagnetic interaction, the SPC implements a virtual admittance to regulate the current injected into the grid in response to the difference between the electromotive force (emf) of the virtual generator and the voltage at the point of common coupling (PCC). The virtual admittance acts a first-order low pass filter, which enables minimizing the effect of PCC voltage variability, making the system more stable and smoothing the current injected into the grid [14].

The reference current provided by the virtual admittance can be controlled through a standard current control loop. Therefore, a SPC-based power converter acts a grid-connected controlled current source, which inherently avoids the risk of over-current in case of short-circuits and grid faults.

The purpose of this work is to analyse the effect of some relevant parameters on the small-signal stability of a grid-connected SPC-controlled VSC. To do this, a small signal model of the system is initially derived. From this model and applying the linear technique of the participation factors, it is finally observed how the variation of the parameters affects the location of the values of the linearised system.

The remaining part of the paper has been structured as follows. Section II provides a concise and complete description of the system under study. Subsequently in Section III, a system of differential algebraic equations (DAEs) is obtained for each of the parts of the system. These DAEs fully describe the dynamics of the system in the frequency range of interest and, after some algebraic manipulation, are rearranged as a non-linear state-space model. Finally, the non-linear state-space model is linearised at an equilibrium point getting a small-signal model of the system. In Section IV sensitivity analysis is carried out, i.e., variation of the system eigenvalues versus the variation of some of their parameters is observed. Additionally, root locus plots of the system eigenvalues with change of some relevant parameters are obtained in this same section. In Section V some time-domain simulations are performed to confirm the results of the sensitivity analysis of the previous section. Finally, Section VI draws the main conclusions from the work.

II. System overview

Fig. 1 shows a schematic diagram of the system under study, consisting of a three-phase grid-connected SPC-controlled VSC. Although VSCs are connected to the grid through filters that in general are more complex than a simple L-filter, in order to simplify the analysis, only this type of filter has been considered in this work.

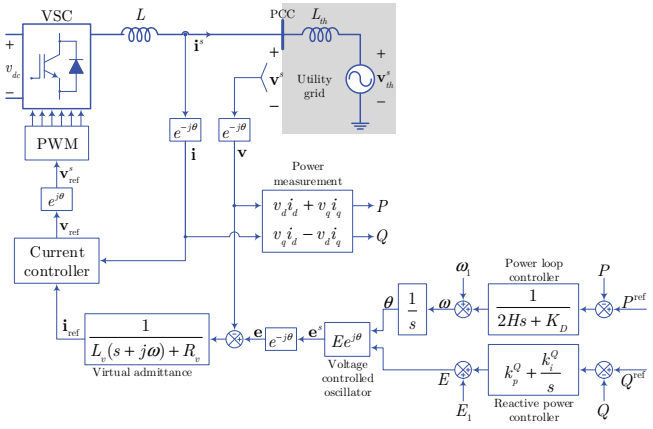

Fig. 1: Three-phase SPC-controlled grid-connected VSC.

For simplifying the analysis, the following assumptions have been made: the terminals voltage at the DC bus, v_{dc}, has been assumed constant; balanced three-phase conditions have been assumed for voltages and currents, i.e. they contain only positive sequences; the VSC switching dynamics has been neglected and only an ideal averaged model is assumed for the converter.

In this work, boldface letters are used to denote complex space vectors. Vectors referred to the $\alpha\beta$-frame are denoted with the superscript s, whereas their counterparts in dq-frame are represented without this superscript.

III. Mathematical modelling of the system

In this section, a state-space model of the system has been obtained. For this, a system of differential equations is firstly obtained. These DAEs fully describe the dynamics of the system in the frequency range of interest and, after some algebraic manipulation, are rearranged as a non-linear state-space model. Finally, the non-linear state-space model is linearised at an equilibrium point getting a small-signal model of the system.

A. Power loop controller (PLC)

Active power control is carried out by means of the power PLC block that relates the input and the output signals by (1), where where H [s] and K_D [pu] are the inertia and the damping coefficient of the virtual generator, and ω_1 y ω [pu] are the fundamental frequency and the frequency of the virtual generator respectively.

$$\left(P^{\text{ref}} - P\right)\frac{1}{2Hs + K_D} + \omega_1 = \omega \tag{1}$$

The relation (1) can be expressed in the time domain by means of (2) where $\Delta\omega = \omega - \omega_1$ and $\Delta P = P - P^{\text{ref}}$.

$$\frac{d\Delta\omega}{dt} = -\frac{K_D}{2H}\Delta\omega - \frac{1}{2H}\Delta P \tag{2}$$

On the other hand, as it is shown in in Fig. 1 the angle θ determines the rotor position of the VSM and it is obtained by integrating the angular frequency ω and therefore,

$$\frac{d\theta}{dt} = \omega \tag{3}$$

B. Reactive power control (RPC)

Reactive power control is carried out by means of a PI controller that relates the input and output signals by means of (4) where E_1 and E [pu] are the nominal voltage and the value of the emf of the the virtual generator.

$$\left(Q^{\text{ref}} - Q\right)\left(k_p^Q + \frac{k_i^Q}{s}\right) + E_1 = E \tag{4}$$

A state space representation of (4) is given by (5) where $\Delta E = E - E_1$ and $\Delta Q = Q - Q^{\text{ref}}$.

$$\begin{aligned} \frac{d\eta}{dt} &= -k_i^Q \Delta Q \\ \Delta E &= \eta - k_p^Q \Delta Q \end{aligned} \tag{5}$$

C. Voltage controller oscillator (VCO)

The VCO block has as inputs the voltage E and phase θ from which it generates a sinusoidal virtual efm that is naturally expressed in the $\alpha\beta$-frame as

$$\mathbf{e}^s = e_\alpha + je_\beta = Ee^{j\theta} \tag{6}$$

Since the virtual admittance and the current control has been implemented in a dq synchronous reference frame (SRF) sets by the angular position of the rotor of the VSM, the change of (6) from $\alpha\beta$ ot dq is given by

$$\mathbf{e} = e_d + je_q = \mathbf{e}^s e^{-j\theta} \tag{7}$$

D. Virtual admittance

In the $\alpha\beta$-frame the virtual admittance transfer function is given by

$$Y^s(s) = \frac{1}{L_v s + R_v} \tag{8}$$

However, it should be noted that a relation $\mathbf{y}^s = G^s(s)\,\mathbf{u}^s$ in $\alpha\beta$ gives a frequency translation $s \to s + j\omega$ in dq [15, 16], i.e., $\mathbf{y} = G^s(s + j\omega)\mathbf{u}$. Therefore, the difference between the emf $\mathbf{e}$ and the PCC voltage $\mathbf{v}$ and the current reference $\mathbf{i}_{\text{ref}}$ are related in dq-frame by means of

$$\mathbf{i}_{\text{ref}} = \frac{1}{L_v(s + j\omega) + R_v}(\mathbf{e} - \mathbf{v}) \tag{9}$$

which becomes

$$L_v \frac{d\mathbf{i}_{\text{ref}}}{dt} = \mathbf{e} - \mathbf{v} - R_v \mathbf{i}_{\text{ref}} - j\omega L_v \mathbf{i}_{\text{ref}} \tag{10}$$

when is expressed in the time domain.

E. Current control

Considering that the dynamics of the current control are relatively fast compared to the dynamics of the external control loops, the entire current control can be simplified to a first order system such as (11), where τ is the desired time-constant.

$$\mathbf{i} = \frac{1}{\tau s + 1}\mathbf{i}_{\text{ref}} \tag{11}$$

that can be expressed in the time domain as

$$\frac{d\mathbf{i}}{dt} = -\frac{1}{\tau}\mathbf{i} + \frac{1}{\tau}\mathbf{i}_{\text{ref}} \tag{12}$$

F. External grid

The system is connected to the grid at the PCC. In order to simplify the analysis, the entire AC system has been replaced by its Thevenin equivalent consisting of a voltage source $\mathbf{v}_{th}$ in series with a inductance L_{th}.

The voltage at the point of common coupling is given in the dq-frame by

$$\mathbf{v} = \mathbf{v}_{th} + L_{th}\frac{d\mathbf{i}}{dt} + jL_{th}\omega\mathbf{i} \tag{13}$$

and L_{th} [pu] can be calculated by (14) where the short circuit ratio (SCR) measures the strength of the AC system with regard to a VSC [17].

$$L_{th} = \frac{1}{\text{SCR}} \tag{14}$$

G. Active and reactive power measurement

The active and reactive power measurements, P and Q, are obtained by means of the relations

$$\begin{aligned} P &= v_d i_d + v_q i_q \\ Q &= v_q i_d - v_d i_q \end{aligned} \tag{15}$$

H. State-space representation of the system

Equations obtained in the previous subsections shape a differential-algebraic system of equations (DAEs) that can be expressed in the classical form

$$\begin{aligned} \dot{\mathbf{x}} &= \mathbf{f}(\mathbf{x}, \mathbf{u}) \\ \mathbf{y} &= \mathbf{g}(\mathbf{x}, \mathbf{u}) \end{aligned} \tag{16}$$

In order to apply linear analysis techniques, such as sensitivity analysis (16) has been linearized and expressed in the form

$$\begin{aligned} \Delta\dot{\mathbf{x}} &= \mathbf{A}\Delta\mathbf{x} + \mathbf{B}\Delta\mathbf{u} \\ \Delta\mathbf{y} &= \mathbf{C}\Delta\mathbf{x} + \mathbf{D}\Delta\mathbf{u} \end{aligned} \tag{17}$$

where

$$\begin{aligned} \Delta\mathbf{x} &= \begin{bmatrix} \Delta\omega & \Delta\theta & \Delta\eta & \Delta i_d^{\text{ref}} & \Delta i_q^{\text{ref}} & \Delta i_d & \Delta i_q \end{bmatrix}^T \\ \Delta\mathbf{y} &= \begin{bmatrix} \Delta P & \Delta Q \end{bmatrix}^T \\ \Delta\mathbf{u} &= \begin{bmatrix} \Delta P^{\text{ref}} & \Delta Q^{\text{ref}} \end{bmatrix}^T \end{aligned} \tag{18}$$

For reasons of space, matrices $\mathbf{A}$, $\mathbf{B}$, $\mathbf{C}$ and $\mathbf{D}$ have not been included in the document.

IV. Sensitivity analysis

Once a state-space model has been obtained, the influence of the different parameters on the location of the eigenvalues of the system is graphically observed in this section. At the same time, the graphic information is corroborated by means of a sensitivity analysis.

Sensitivity analysis shows how the variation of the system parameters affects the location of the eigenvalues [18]. The sensitivity s_β^i of the eigenvalue λ_i to parameter β is provided by

$$s_\beta^i = \frac{d\lambda_i}{d\beta} = \frac{\boldsymbol{\Psi}_i \dfrac{\partial \mathbf{A}}{\partial \beta}\boldsymbol{\Phi}_i}{\boldsymbol{\Psi}_i \boldsymbol{\Phi}_i} \tag{19}$$

where $\boldsymbol{\Psi}_i$ and $\boldsymbol{\Phi}_i$ are the left and right eigenvalues associated to the eigenvalue λ_i [19]. Although sensitivities are generally complex numbers, it is its real parts that determine the stability of the system [20] and they are the only ones considered in this analysis.

TABLE I: VSC specifications

Quantity	Symbol	Value
Rated power	S_n	125 kVA
AC voltage	V_n	400 V
DC voltage	v_{dc}	750 V
AC frequency	f	50 Hz
Switching frequency	f_{sw}	3150 Hz
L-filter inductance	L	1180 µH

Eigenvalue	ζ	f (Hz)	Sensitivity				
			s^i_{scr}	s^i_H	$s^i_{K_D}$	$s^i_{k_p^Q}$	$s^i_{k_i^Q}$
$\lambda_{1,2}$=−1333.8±j8.9	1	1.42	89.278	−0.002	0	−276.819	0.204
$\lambda_{3,4}$= −48.3±j301.7	0.16	48.02	−3.278	0.077	0	94.000	0.852
λ_5= −13.0±j0	1	0	−0.143	5.899	−0.227	23.773	−1.829
$\lambda_{6,7}$= −9.9±j5.4	0.88	0.86	−0.136	2.697	−0.012	−1.246	−0.141

TABLE II: Eigenvalues and sensitivities of SPC

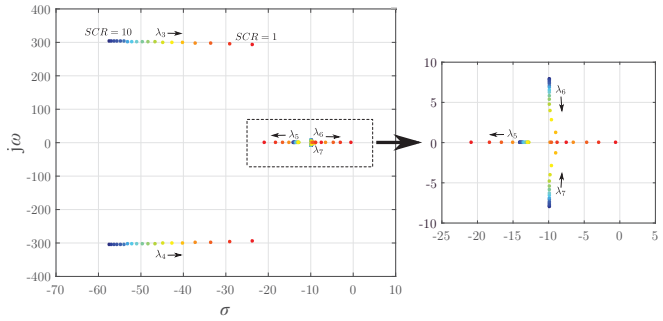

Fig. 2: Eigenvalues for a sweep of SCR from 10 to 1.

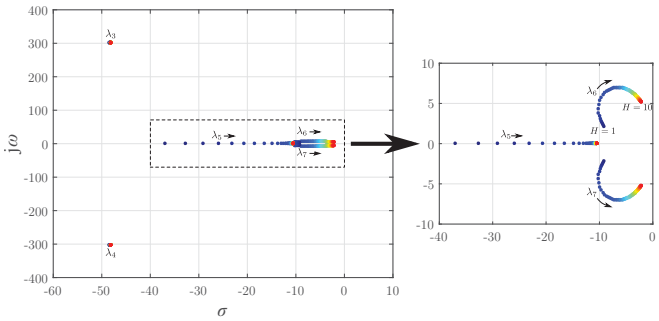

Fig. 3: Eigenvalues for a sweep of H from 1 s to 10 s.

The VSC specifications is shown in Tables I. For all the graphs, the operation point is given by $P_0 = 0.8$ pu and $Q_0 = 0.8$ pu. Eigenvalues and sensitivities of the system are showed in Table II for SCR = 10, $P_0 = 0.8$ pu and $Q_0 = 0.8$ pu.

Although the resulting system (17) is of seventh order, some of the eigenvalues are too far away in the left half-plane and therefore is neglected. The remaining ones are the dominant eigenvalues.

A. Influence of the SCR

Fig. 2 shows the eigenvalues of the system for a sweep of the SCR from 10 to 1. The arrows points in the direction in which the SCR decreases. It can be seen that as the SCR decrease, the conjugated complex eigenvalues $\lambda_{6,7}$ become real and move toward the right decreasing the relative stability of the system and showing a very slow response in the time domain.

This is confirmed by the sensitivity values in Table II according to which the sensitivity s^i_{scr} for the eigenvalues $\lambda_{6,7}$ and the variation of the SCR are of opposite sign.

B. Influence of the inertia constant H

Fig. 3 shows the eigenvalues of the system for a sweep of H from 1 to 10. The arrows show direction in which the H increases. It can be seen that as H increases, the conjugated complex eigenvalues $\lambda_{6,7}$ move to the right producing a slow oscillatory response in the time domain.

This is confirmed by the sensitivity values in Table II according to which the sensitivity s^i_H for the eigenvalues $\lambda_{6,7}$ and the variation of the H are of same sign.

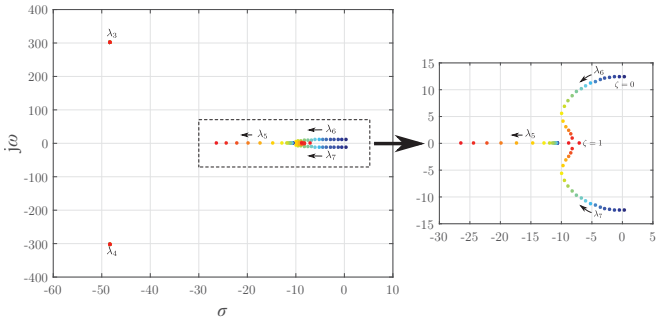

Fig. 4: Eigenvalues for a sweep of ζ from 0 to 1.

C. Influence of the damping constant K_D

Fig. 4 shows the eigenvalues of the system for values of K_D equivalent to a sweep of the damping values ζ from 0 to 1. The arrows show direction in which the ζ increases. It can be seen that for $\zeta \approx 0$ the location of the conjugated complex eigenvalues $\lambda_{6,7}$ shows a totally oscillatory behavior. As ζ increases, these eigenvalues become real which indicates an over damped response.

This is confirmed by the sensitivity values in Table II according to which the sensitivity $s^i_{K_D}$ for the eigenvalues $\lambda_{6,7}$ and the variation of the K_D are of opposite sign.

D. Influence of the k_p^Q constant of the Q controller

Fig. 5 shows the eigenvalues of the system for a sweep of k_p^Q from 0 to 0.72. The arrows show direction in which the k_p^Q increases. It can be seen that the conjugated complex eigenvalues $\lambda_{3,4}$ shows a oscillatory behavior that increases as the value of k_p^Q increases until the system becomes unstable.

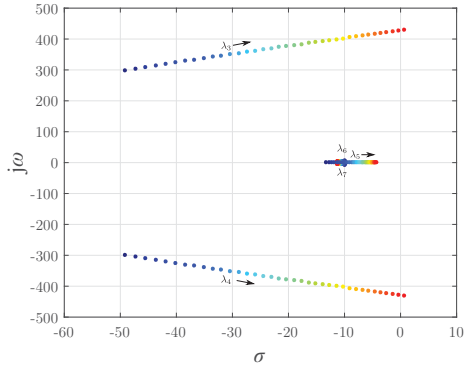

Fig. 5: Eigenvalues for a sweep of k_p^Q from 0 to 0.72.

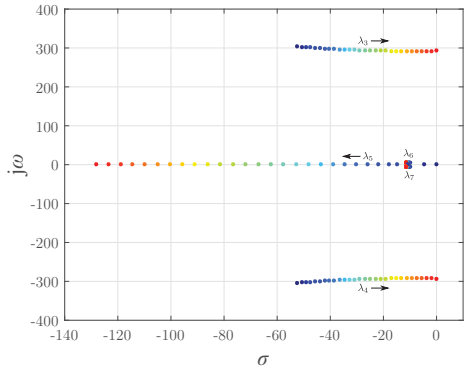

Fig. 6: Eigenvalues for a sweep of k_i^Q from 0 to 56.

This is confirmed by the sensitivity values in Table II according to which the sensitivity $s^i_{k_p^Q}$ for the eigenvalues $\lambda_{3,4}$ and the variation of the k_p^Q are of opposite sign.

E. Influence of the k_i^Q constant of the Q controller

Fig. 6 shows the eigenvalues of the system for a sweep k_i^Q from 0 to 56. The arrows show direction in which the k_i^Q increases. As in the case of k_p^Q, it can be seen that the conjugated complex eigenvalues $\lambda_{3,4}$ shows a oscillatory behavior that increases as the value of k_i^Q increases until the system becomes unstable.

This is confirmed by the sensitivity values in Table II according to which the sensitivity $s^i_{k_i^Q}$ for the eigenvalues $\lambda_{3,4}$ and the variation of the k_i^Q are of opposite sign.

V. Simulations

Some time-domain simulations were performed in Simulink to confirm the results of the sensitivity analysis in the previous section as can be observed in Fig. 7. In Fig. 7a can be observed the time step response for two different values of H. For $H = 10$ the response of the system is slower than for $H = 2$. In the same way in Fig. 7b it is observed that for $\zeta = 0.1$ the response is oscillating while for $\zeta = 0.7$ the response is more damped. These results are as expected according to the analysis of Section IV.

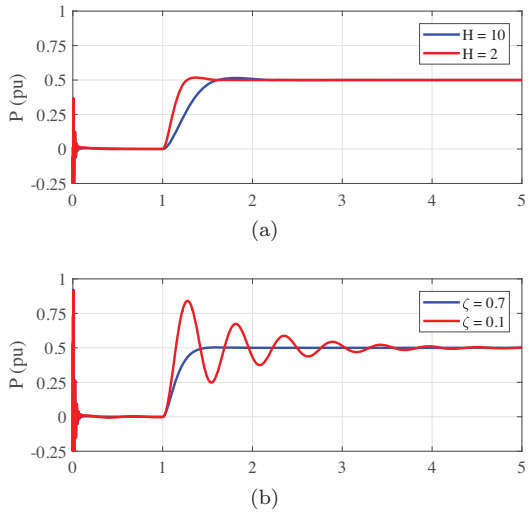

Fig. 7: Time response of the system: $\Delta P = 0.5\,\text{pu}$ at $t = 1\,\text{s}$.

VI. Conclusions

In this work, a sensitivity analysis of a three-phase grid-connected SPC-controlled VSC SPC has been carried out. Firstly, a non-linear mathematical model of the system has been developed. This non-linear model has been linearized obtaining a small signal model from which plots of the system eigenvalues sweeping different parameters have been made. To confirm the graphical analysis, the system sensitivities have been calculated. Finally, time domain simulations are performed to confirm the results of the sensitivity analysis.

It is important to note that the eigenvalues of the system follow a pattern similar to that of a SM. This should not be surprising since the SPC aims precisely to emulate the behavior of a SM. However, unlike the real SG in which its parameters are fixed, in the SPC its parameters are adaptive to different operating conditions of the system. In this sense, this work makes it possible to accurately predict the limits within which system parameters can vary to ensure stable operation of the system.

Acknowledgment

This work was partially supported by the European Commission under project FLEXITRANSTORE - H2020-LCE-2016-2017-SGS-774407 and by the Spanish Ministry of Science under project ENE2017-88889-C2-1-R.

References

[1] World Energy Council, "Variable renewables integration in electricity systems: how to get it right," *World Energy Perspectives*, 2016.

[2] L. Marin, P. Rodriguez, I. Candela, and J. Rocabert, "A way of increasing stability margin of current control in vscs connected to the grid through lcl filters," in *2017 IEEE Energy Conversion Congress and Exposition (ECCE)*, Oct 2017, pp. 4983–4988.

[3] D. Eltigani and S. Masri, "Challenges of integrating renewable energy sources to smart grids: A review," *Renewable and Sustainable Energy Reviews*, vol. 52, pp. 770–780, 2015.

[4] E.-E. AISBL, "Entso-e network code for requirements for grid connection applicable to all generators," *ENTSO-E AISBL: Brussels, Belgium*, 2012.

[5] M. Abdollahi, J. I. Candela, J. Rocabert, R. S. M. Aguilar, and P. Rodriguez, "Analysis on dynamic interaction of renewable SSG SPC with external power grid," in *2017 IEEE 6th International Conference on Renewable Energy Research and Applications (ICRERA)*, Nov 2017, pp. 1067–1072.

[6] H.-P. Beck and R. Hesse, "Virtual synchronous machine," in *9th International Conference on Electrical Power Quality and Utilisation*. Barcelona: IEEE, Oct 2007, pp. 1–6.

[7] Q.-C. Zhong and G. Weiss, "Synchronverters: Inverters that mimic synchronous generators," *IEEE Transactions on Industrial Electronics*, vol. 58, no. 4, pp. 1259–1267, 2011.

[8] S. D'Arco and J. A. Suul, "Virtual synchronous machines classification of implementations and analysis of equivalence to droop controllers for microgrids," in *PowerTech*. Grenoble: IEEE, Jun 2013, pp. 1–7.

[9] J. Roldan-Perez, A. Rodríguez-Cabero, and M. Prodanovic, "Harmonic virtual impedance design for a synchronverter-based battery interface converter," in *2017 IEEE 6th International Conference on Renewable Energy Research and Applications (ICRERA)*, Nov 2017, pp. 774–779.

[10] P. Rodriguez, I. Candela, and A. Luna, "Control of PV generation systems using the synchronous power controller," in *2013 IEEE Energy Conversion Congress and Exposition*. Denver: IEEE, Sept 2013, pp. 993–998.

[11] C. Verdugo, J. I. Candela, and P. Rodriguez, "Grid support functionalities based on modular multilevel converters with synchronous power control," in *2016 IEEE International Conference on Renewable Energy Research and Applications (ICRERA)*, Nov 2016, pp. 572–577.

[12] M. Abdollahi, J. I. Candela, J. Rocabert, R. S. M. Aguilar, and P. Rodriguez, "Active power limiter for grid connection of modern renewable SSG SPC," in *2017 IEEE 6th International Conference on Renewable Energy Research and Applications (ICRERA)*, Nov 2017, pp. 728–733.

[13] D. Remon, W. Zhang, A. Luna, I. Candela, and P. Rodriguez, "Grid synchronization of renewable generation systems using synchronous power controllers," in *2017 IEEE 6th International Conference on Renewable Energy Research and Applications (ICRERA)*, Nov 2017, pp. 169–174.

[14] A. Tarraso, J. I. Candela, J. Rocabert, and P. Rodriguez, "Grid voltage harmonic damping method for spc based power converters with multiple virtual admittance control," in *2017 IEEE Energy Conversion Congress and Exposition (ECCE)*, Oct 2017, pp. 64–68.

[15] K. Sharifabadi, L. Harnefors, H. Nee, S. Norrga, and R. Teodorescu, *Design, control, and application of modular multilevel converters for HVDC transmission systems*. John Wiley & Sons, 2016.

[16] L. Harnefors, "Modeling of three-phase dynamic systems using complex transfer functions and transfer matrices," *IEEE Transactions on Industrial Electronics*, vol. 54, no. 4, pp. 2239–2248, Aug 2007.

[17] "*IEEE Guide for Planning DC Links Terminating at AC Locations Having Low Short-Circuit Capacities*," IEEE Std 1204-1997(R2003), Jan 1997.

[18] S. D'Arco, J. A. Suul, and O. B. Fosso, "Control system tuning and stability analysis of virtual synchronous machines," in *2013 IEEE Energy Conversion Congress and Exposition*, Sept 2013, pp. 2664–2671.

[19] P. Kundur, *Power System Stability and Control*, ser. The EPRI Power System Engineering Series. New York: McGraw-Hill, Inc., 1994.

[20] S. D'Arco, J. A. Suul, and O. B. Fosso, "A virtual synchronous machine implementation for distributed control of power converters in smartgrids," *Electric Power Systems Research*, vol. 122, pp. 180–197, 2015.